5194 J. Agric. Food Chem. **2009,** *57,* 5194–5200
DOI:10.1021/jf9005593

JOURNAL OF
AGRICULTURAL AND
FOOD CHEMISTRY
ARTICLE

β-Triketone Inhibitors of Plant *p*-Hydroxyphenylpyruvate Dioxygenase: Modeling and Comparative Molecular Field Analysis of Their Interactions

Franck E. Dayan,*,† Nidhi Singh,‡ Christopher R. McCurdy,‡
Colette A. Godfrey,§,# Lesley Larsen,§,# Rex T. Weavers,#
John W. Van Klink,§,# and Nigel B. Perry§,#

†Natural Products Utilization Research Unit, Agricultural Research Service, U.S. Department of Agriculture, P.O. Box 8048, University, Mississippi 38677, ‡Department of Medicinal Chemistry, University of Mississippi, University, Mississippi 38677, §New Zealand Institute for Plant and Food Research Ltd. and #Department of Chemistry, University of Otago, P.O. Box 56, Dunedin, New Zealand

p-Hydroxyphenylpyruvate dioxygenase (HPPD) is the target site of β-triketone herbicides in current use. Nineteen β-triketones and analogues, including the naturally occurring leptospermone and grandiflorone, were synthesized and tested as inhibitors of purified *Arabidopsis thaliana* HPPD. The most active compound was a β-triketone with a C_9 alkyl side chain, not reported as natural, which inhibited HPPD with an I_{50} of 19 ± 1 nM. This is significantly more active than sulcotrione, which had an I_{50} of 250 ± 21 nM in this assay system. The most active naturally occurring β-triketone was grandiflorone, which had an I_{50} of 750 ± 70 nM. This compound is of potential interest as a natural herbicide because it can be extracted with good yield and purity from some *Leptospermum* shrubs. Analogues without the 1,3-diketone group needed to interact with Fe^{2+} at the HPPD active site were inactive (I_{50}s > 50 μM), as were analogues with prenyl or ethyl groups on the triketone ring. Modeling of the binding of the triketones to HPPD, three-dimensional QSAR analysis using CoMFA (comparative molecular field analysis), and evaluation of the hydrophobic contribution with HINT (hydropathic interactions) provided a structural basis to describe the ligand/receptor interactions.

KEYWORDS: Natural products; triketones; phytotoxins; herbicides; mode of action; *p*-hydroxyphenylpyruvate dioxygenase; structure–activity relationships; essential oils

INTRODUCTION

p-Hydroxyphenylpyruvate dioxygenase (HPPD; EC 1.13.11.27, EC 1.14.2.2) is a nonheme, iron II containing, α-keto acid-dependent enzyme that catalyzes the formation of homogentisic acid (HGA). This mechanistically complex reaction involves the oxidative decarboxylation of the 2-oxoacid side chain of 4-hydroxyphenylpyruvate (4-HPP), the subsequent hydroxylation of the aromatic ring, and a 1,2 (ortho) rearrangement of the carboxymethyl group (*1*–*3*).

In plants, HGA is a key precursor in the biosynthesis of tocochromanols (tocopherols and tocotrienols) and prenylquinones. The prenylquinone plastoquinone is an essential cofactor for phytoene desaturase (*4*). Inhibition of HPPD causes photodynamic bleaching of the foliage because the reduction of plastoquinone levels hampers phytoene desaturase activity (*5*). Under high light intensity, the reduced pool of carotenoids within the thylakoid membranes no longer quenches the excess energy, destabilizing the photosynthetic apparatus, which leads to a rapid degradation of chlorophylls.

HPPD is the molecular target site for β-triketone herbicides in current use, for example, sulcotrione, mesotrione, and tembotrione (*5*–*11*). This class of herbicides was inspired by the natural β-triketone phytotoxin leptospermone (**4**, **Figure 1**) produced by the bottlebrush plant (*Callistemon* spp.) (*7*, *12*, *13*). β-Triketones are also found in other Australasian woody plants in the family Myrtaceae, for example, *Leptospermum*, *Eucalyptus*, and *Corymbia* (*14*–*17*). β-Triketones, and essential oils rich in these compounds, have a variety of biological activities (*18*): antifungal and antimicrobial (*19*–*22*), antiviral (*21*, *23*), insecticidal and molluscicidal (*21*), and herbicidal (*13*, *24*, *25*).

The structure–activity relationship (SAR) of synthetic β-triketones against HPPD has been extensively pursued, leading to the design of several successful commercial herbicides [e.g., sulcotrione (2-[2-chloro-4-methanesulfonylbenzoyl]cyclohexane-1,3-dione) and mesotrione (2-[4-methylsulfonyl-2-nitrobenzoyl]cyclohexane-1,3-dione)] (*5*–*9*). We recently reported that natural β-triketones leptospermone **4** and grandiflorone **6** (**Table 1**), from the essential oil of manuka (*Leptospermum scoparium*), inhibited HPPD (*25*). However, in contrast to their synthetic counterparts, these compounds were competitive, reversible inhibitors (*25*). A series of β-triketones has been synthesized and tested for their antimicrobial activity (*19*), and we now report the activity of 15 of these compounds, plus four new analogues, against HPPD. Modeling of their interaction with the catalytic site of HPPD and three-dimensional quantitative structure–activity

---

*Author to whom correspondence should be addressed [telephone (662) 915 1039; fax (662) 915 1035; e-mail fdayan@olemiss.edu].

Published on Web 05/12/2009
© 2009 American Chemical Society

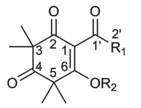

N	R1	R2
1	methyl	H
2	1-methylethyl	H
3	benzyl	H
4	2-methylpropyl	H
5	1-methylpropyl	H
6	2-phenethyl	H
7	pentyl	H
8	cyclohexyl	H
9	2-cyclohexylethyl	H
10	2-cyclohexylethyl	methyl
11	nonyl	H
12	undecyl	H
13	pentadecyl	H

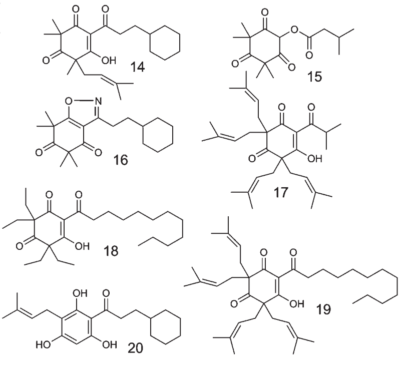

Figure 1. Structures of the β-triketones and related compounds tested in this study.

relationship analysis with comparative molecular field analysis (CoMFA) were used to explain the activity of these natural herbicides and analogues.

MATERIALS AND METHODS

General Experimental Procedures. All solvents were distilled before use and were removed by rotary evaporation at temperatures up to 35 °C. Merck silica gel 60, 200−400 mesh, 40−63 μm, was used for silica gel flash chromatography. TLC was carried out using Merck DC-plastikfolien Kieselgel 60 F254, visualized with a UV lamp. High-resolution mass, UV, and IR spectra were recorded on Kratos MS-80 (EI) or Bruker micro Q-TOF (ESI), Shimadzu UV 240, and Perkin-Elmer 1600 FTIR instruments, respectively. NMR spectra, at 25 °C, were recorded at 300 MHz for ^{1}H and at 75 MHz for ^{13}C on a Varian INOVA 300 spectrometer. Chemical shifts are given in parts per million on the δ scale referenced to the solvent peaks $CHCl_3$ at 7.25 ppm and $CDCl_3$ at 77.0 ppm.

Syntheses. All of the compounds were prepared as described previously (*19*), except for **10** and **14**−**16**, which were synthesized as described below. Structural assignments were made by comparison with previously synthesized compounds (*19*) and/or additional 2D NMR experiments to confirm connectivities.

Compound 10. β-Triketone **9** (100 mg, 0.31 mmol) and silver oxide (50 mg, 0.22 mmol) were refluxed for 5 h with MeI (2.5 mL). The MeI was left to evaporate and the residue taken up in CH_2Cl_2 and filtered through Celite. Column chromatography with CH_2Cl_2/EtOAc (1:0 to 5:1) gave the O-methylated product **10** as an amorphous white solid (50 mg, 0.15 mmol, 48%): IR (film) ν_{max} 2982, 2925, 2852, 1723, 1672, 1558, 1472, 1449, 1382, 1049 cm^{-1}; UV (MeOH) λ_{max} (log ε) 278 (4.2) nm; HREIMS (70 eV) *m*/*z* (rel int) 334.2132 [M]$^+$ (2%, 334.2144 calcd for $C_{20}H_{30}O_4$), 319 (30), 223 (100), 191 (44), 168 (70); ^{1}H NMR ($CDCl_3$, 300 MHz) δ 0.89 (2H, m, H-5′ + H-9′), 1.16 (2H, m, H-6′ + H-8′), 1.24 (1H, m, H-4′), 1.35 (6H, s, 5-Me), 1.40 (6H, s, 3-Me), 1.53 (2H, m, H-3′), 1.60 (2H, m, H-6′ + H-8′), 1.62 (2H, m, H-7′), 1.68 (2H, m, H-5′ + H-9′), 2.73 (2H, t, J = 7 Hz, H-2′), 4.77 (3H, s, 6-O-Me); ^{13}C NMR ($CDCl_3$, 75 MHz) δ 23.9 (3-Me), 25.3 (5-Me), 26.2 (C-6′ + C-8′), 26.5 (C-7′), 33.1 (C-5′ + C-9′), 31.4 (C-3′), 37.2 (C-4′), 42.9 (C-2′), 49.6 (C-3), 55.6 (C-5), 61.3 (6-O-Me), 117.5 (C-1), 174.8 (C-6), 198.7 (C-2), 205.5 (C-1′), 211.1 (C-4).

Compound 14. To the 2-cyclohexylethyl phloroglucinol described previously (*19*) (500 mg, 1.9 mmol) in acetone (5 mL) was added K_2CO_3 (240 mg, 1.74 mmol) and prenyl bromide (0.2 mL, 1.9 mmol). The mixture was heated at reflux for 4 h, acidified with HCl (3 M) and extracted with EtOAc. The solvent was then removed to give a yellow residue. Column chromatography on silica gel with CH_2Cl_2/EtOAc gave the monoprenylated product phloroglucinol **20** as a yellow gum (200 mg, 0.6 mmol, 32%): HR-ESIMS *m*/*z* 333.2038 [M + H]$^+$ (333.2060 calcd for $C_{20}H_{29}O_4$); ^{1}H NMR ($CDCl_3$, 300 MHz) δ 1.03 + 1.82 (m, H-5′ + H-9′), 1.21 (m, H-4′), 1.29 + 1.70 (m, H-6′ + H-8′), 1.56 (m, H-3′), 1.74 (m, H-7′), 1.71 (s, H-5″), 1.78 (s, H-4″), 3.04 (t, J = 7 Hz, H-2′), 3.31 (d, J = 7 Hz, H-1″), 5.21 (t, J = 7 Hz, H-2″), 6.15 (s, H-3), 9.34 (s, 4-OH), 12.19 (s, 6-OH), 14.29 (s, 2-OH). To this monoprenylated 2-cyclohexylethyl phloroglucinol **20** (200 mg, 0.6 mmol) in NaOMe (380 mg of Na in 5 mL of MeOH) was added MeI (5 mL). The reaction mixture was heated at reflux for 2 h, acidified with HCl (3 M), and extracted with EtOAc. Separation, drying, and removal of organic solvent gave an orange residue. Column chromatography on silica gel using CH_2Cl_2 gave the methylated product **14** as a colorless gum (80 mg, 0.21 mmol, 36%): IR (film) ν_{max} 2980, 2925, 2852, 1719, 1672, 1560, 1450, 1379, 1034 cm^{-1}; UV (MeOH) λ_{max} (log ε) 278, (4.0), 230 (3.8) nm; HR-ESIMS *m*/*z* 375.2525 [M + H]$^+$ (375.2530 calcd for $C_{23}H_{35}O_4$). NMR spectra of **14** showed two tautomers (approximate ratio 3:2): ^{1}H NMR ($CDCl_3$, 300 MHz) δ 1.24 (m, H-4′), 1.30 + 1.29 + 1.26 (m, 3-Me), 1.44 + 1.40 + 1.39, (m, 5-Me), 1.49 + 1.17 (m, H-6′ + H-8′), 1.49 (m, H-3′), 1.60 + 1.56 (m, H-4″) + 1.52 + 1.47 (m, H-5″), 1.66 + 0.93 (m, H-5′ + H-9′), 1.71 (m, H-7′), 2.52 (m, H-1″), 2.98 (m, H-2′), 4.76 (m, H-2″), 18.34 (s, 2-OH); ^{13}C NMR ($CDCl_3$, 75 MHz) major tautomer δ 17.8 (C-5″), 20.3 (3/5-Me), 22.3 (3/5-Me), 25.8 (C-4″), 26.1 (3/5-Me), 26.2 (C-6′ + C-8′), 26.5 (C-7′), 32.4 (C-3′), 33.1 (C-5′ + C-9′), 37.1 (C-4′), 37.5 (C-2′), 38.9 (C-1″), 51.9 (C-3), 57.2 (C-5), 110.8 (C-1), 118.0 (C-2″), 137.1 (C-3″), 196.5 (C-6), 197.7 (C-2), 205.1 (C-1′), 210.2 (C-4); minor tautomer δ 17.9 (C-5″), 20.8 (3/5-Me), 22.2 (3/5-Me), 25.9 (C-4″), 26.1 (3/5-Me), 26.2 (C-6′ + C-8′), 26.5 (C-7′), 32.4 (C-3′), 33.1 (C-5′ + C-9′), 37.0 (C-4′), 37.5 (C-2′), 38.0 (C-1″), 51.4 (C-3), 56.1 (C-5), 110.1 (C-1), 117.5 (C-2″), 135.8 (C-3″), 196.2 (C-6), 199.1 (C-2), 205.0 (C-1′), 209.8 (C-4).

Table 1. In Vitro Inhibition of *p*-Hydroxyphenylpyruvate Dioxygenase by β-Triketones and Selected Calculated Properties

compd	natural product name	I_{50}[a] (nM ± 1 SE)	pI_{50}	Clog P[b]	HINT log P[c]	volume[d] (Å^3)	binding energy[e]
1		>50000	<4.3	1.13	0.25	201.8	−42.1
2	flavesone	44500 ± 4000	4.35	1.97	1.34	234.3	−55.9
3		18900 ± 1800	4.72	2.87	1.81	270.2	−34.1
4	leptospermone	11800 ± 1000	4.93	2.58	1.88	254.8	−27.9
5	isoleptospermone	14300 ± 1200	4.84	2.49	1.88	252.7	−51.8
6	grandiflorone	750 ± 70	6.13	3.22	2.35	284.9	−35.0
7	papuanone	960 ± 100	6.02	3.24	2.42	269.1	−19.1
8		>50000	<4.3	3.16	2.77	275.8	−60.4
9		170 ± 20	6.77	4.31	3.73	310.9	−32.0
10		410 ± 50	6.39	4.78	4.43	325.4	−85.1
11		19 ± 1	7.72	5.36	4.58	336.1	−24.5
12		250 ± 50	6.60	6.42	5.66	369.4	−36.6
13		310 ± 10	6.51	8.53	7.82	435.8	−12.6
14		2270 ± 280	5.64	5.81	5.21	376.1	−26.1
15		>50000	<4.3	2.86	2.05	258.5	−5.2
16		>50000	<4.3	4.79	3.89	303.5	−3.9
17		>50000	<4.3	7.97	7.82	438.9	>10^6
18		>50000	<4.3	8.53	7.26	494.5	>10^6
19		>50000	<4.3	11.85	11.58	639.3	>10^6
	sulcotrione	250 ± 21	6.60	0.92	0.20	243.3	

[a] I_{50} = concentration required for 50% inhibition HPPD ± standard error. [b] Calculated with ChemBioDraw Ultra, version 11.1. [c] Calculated with Sybyl/HINT, see ref (*33*). [d] Total volume calculated using fast Connolly algorithm. Volume of cyclic triketone moieties: **1**−**9** and **11**−**13**, 184.7; **10,** 199.2; **14**, 244.7; **18**, 254.2; **17** and **19**, 438.3 Å^3. [e] Energy of ligand/receptor interaction in kcal/mol calculated by Sybyl/Flexidock.

Compound 15. H_2O_2 (30%, 1.0 mL) was added to leptospermone **4** (100 mg, 0.38 mmol) suspended in dioxane (1.5 mL) and stirred at room temperature for 24 h. The reaction mixture was diluted with H_2O and extracted with CH_2Cl_2. Semipreparative HPLC (see below) gave unreacted leptospermone and the new compound **15** as an amorphous white solid (22 mg, 0.05 mmol, 14%, 0.39 mmol): IR (film) ν_{max} 2961, 2875, 1767, 1721, 1615, 1470, 1385, 1181, 1094, 1034 cm^{-1}; UV (MeOH) λ_{max} (log ε) 262 (4.0) nm; HREIMS (70 eV) *m*/*z* (rel int) 282.1466 [M]$^+$ (trace, 282.1467 calcd for $C_{15}H_{22}O_5$), 198 (10), 140 (11), 85 (100), 57 (100); ^{1}H NMR ($CDCl_3$, 300 MHz) δ 1.03 (6H, *d*, *J* = 7 Hz, H-4′ + H-5′), 1.40 (12H, br s, 3-Me + 5-Me), 2.16 (1H, m, *J* = 7 Hz, H-3′), 2.42 (2H, d, *J* = 7 Hz, H-2′), 6.04 (1H, s, H-1); ^{13}C NMR ($CDCl_3$, 75 MHz) δ 22.2 (C-4′ + C-5′), 24.3 (3-Me + 5-Me), 25.9 (C-3′), 42.6 (C-2′), 56.3 (C-3 + C-5) 79.9 (C-1), 170.0 (C-1′), 198.7 (C-2 + C-6), 210.8 (C-4); NMR signals assigned from HMBC spectrum.

Semipreparative HPLC was carried out using a Waters system comprising a 717 autosampler, a 600 controller, and a 2487 programmable multiwavelength detector, at 20 °C with a C18 column (Phenomenex Luna ODS(3) 5 μm 100 Å 250 × 10 mm) with a 2 × 4 mm C18 guard column. Peaks were monitored at 210 and 254 nm. The mobile phase was initially 50:50 0.1% formic acid in H_2O/0.1% formic acid in MeCN with a linear gradient over 10 min to 0.1% formic acid in MeCN, with a flow rate of 5 mL min^{-1}, giving compound **15** with a retention time of 7.5 min.

Compound 16. Hydroxylamine hydrochloride (30 mg) and sodium acetate (45 mg, 0.54 mmol) were added to a solution of β-triketone **9** (*19*) (50 mg, 0.16 mmol) in H_2O (1 mL) and ethanol (2 mL). The reaction mixture was heated at reflux for 18 h. Column chromatography on silica gel with CH_2Cl_2 gave the isoxazole **16** as a colorless gum (48 mg, 0.15 mmol, 97%): IR (film) ν_{max} 2981, 2925, 2852, 1724, 1683, 1608, 1474, 1455, 1047 cm^{-1}; UV (MeOH) λ_{max} (log ε) 230 (3.9) nm; HR-ESIMS *m*/*z* 318.2053 $[M + H]^+$ (318.2064 calcd for $C_{19}H_{27}NO_3$); ^{1}H NMR ($CDCl_3$, 300 MHz) δ 0.97 (2H, m, H-5′ + H-9′), 1.19 (2H, m, H-6′ + H-8′), 1.26 (1H, m, H-4′), 1.39 (6H, s, 5-Me), 1.56 (6H, s, 3-Me), 1.59 (2H, overlapped m, H-3′), 1.60 (2H, m, H-6′ + H-8′), 1.62 (2H, m, H-7′), 1.74 (2H, m, H-5′ + H-9′), 2.91 (2H, br t, *J* = 7 Hz, H-2′); ^{13}C NMR ($CDCl_3$, 75 MHz) δ 23.2 (3-Me), 24.0 (C-2′), 25.4(5-Me), 26.2 (C-6′ + C-8′), 26.6 (C-7′), 32.9 (C-5′ + C-9′), 34.7 (C-3′), 37.5 (C-4′), 45.8 (C-3), 57.3 (C-5), 111.4 (C-1), 162.3 (C-2), 181.8 (C-1′), 192.4 (C-6), 211.4 (C-4).

Expression of HPPD and Enzymatic Assays. Recombinant HPPD from *Arabidopsis thaliana* was overexpressed in *Escherichia coli* and purified by immobilized metal affinity chromatography. Enzyme activity was measured as described before (*25*). The HPLC system used to measure enzyme activity was composed of a Waters Corp. system (Milford, MA) that included a model 600E pump, a model 717 autosampler, a Millenium 2010 controller, and a model 996 photodiode detector equipped with a 7.8 mm × 100 mm X-Terra C18 (5 μm) reversed phase column. Solvent A was 0.1% (v/v) trifluoroacetic acid in ddH_2O, and solvent B was 0.08% (v/v) trifluoroacetic acid in 80% (v/v) HPLC-grade acetonitrile/ddH_2O. The solvent system consisted of a linear gradient beginning at 0% (100% A) to 70% B from 0 to 2 min, 70−100% B from 2 to 4 min, 100% B from 4 to 6 min, 100−0% B from 6 to 7 min, and 0% B from 7 to 8 min. The flow rate was 3 mL min^{-1}, and the injection volume was 100 μL. HGA was detected by the UV absorbance at 288 nm (*26*). A calibration curve was established by injecting various concentrations of HGA. Data from dose−response experiments were analyzed using the dose−response curve module (*27*) using R version 2.2.1 (*28*). Mean I_{50} values and standard deviations, obtained using the untransformed data, are given in **Table 1**. The synthetic HPPD inhibitor sulcotrione was included as a positive control (*25*).

Docking of the β-Triketones to HPPD. Molecular modeling was performed using Sybyl v.7.1 software from Tripos Inc. (St. Louis, MO) on a Silicon Graphics Octane 2 workstation, equipped with two parallel R12000 processors. The homology model of *A. thaliana* designed in our previous research (*25*) was used. A subsequent minimization was performed on the transferred ligands with the Tripos force field, as implemented in the Biopolymer module of Sybyl. The root-mean-square (rms) differences between our model and the recently published crystal structure of *A. thaliana* HPPD (*29*) (pdb: 1TG5) was 0.885, indicating the high similarity between the two structures.

The initial structures of β-triketone analogues were derived from the coordinates of leptospermone obtained previously (*25*). Each structure was minimized for 1000 steps each of steepest descent, followed by conjugate gradient, and finally by the BFGS method to a gradient of 0.001 kcal/mol/Å or less. The charges were added to the molecules using the Sybyl Gasteiger−Huckel algorithm. These analogues were docked to the active site of *At*-HPPD using the Flexidock (Genetic algorithm-based flexible docking) routine. FlexiDock explores the conformational and orientational space that defines possible interactions between the ligand and its binding site.

The active site on the *A. thaliana* HPPD was defined as a spherical region of 7 Å radius centered from the β-triketone ligands. This sphere encompasses all residues known to be involved in inhibitor binding (*30*). The default Sybyl/Flexidock parameters were used. Of the several possible conformations obtained for each ligand, the conformation with the lowest binding energy to *At*-HPPD was selected for the CoMFA study.

CoMFA and Prediction of the Inhibitory Activity. CoMFA studies require that the molecules to be analyzed be aligned according to a suitable conformational template, which is assumed to be a “bioactive” conformation (*31*). Therefore, all of the active molecules were “relaxed” within the binding domain of HPPD using MMF94 (*32*). The structures were then aligned along carbons 2, 4, and 6 of their triketone backbone and their 1′ atom (a carbonyl carbon for all the structure, except for **15** and **16**) (**Figure 1**). All analyses were performed using the default lattice parameters for CoMFA consisting of a three-dimensional grid with a width of 2 Å. CoMFA descriptors were calculated using a sp^3 carbon probe atom with a van der Waals radius of 1.5 Å and a charge of +1.0 to generate steric field energies and electrostatic fields with a distance-dependent dielectric at each lattice point. The Sybyl default energy cutoff of 30 kcal/mol was used. The CoMFA steric and electrostatic fields generated were scaled by the CoMFA standard method in Sybyl.

HINT (Hydropathic Interactions) Analysis. The catalytic and substrate binding domain of *A. thaliana* HPPD was extracted from the entire protein by selecting all of the amino acids within a 6 Å radius around **13**, the longest β-triketone present in the data set. The partition coefficient of this domain was calculated using all atoms (including essential hydrogens) and following the partition dictionary for the amino acids available in the HINT (*33*) module of Sybyl. The polar/hydropathic map was then derived by identifying atoms interacting within a 6 Å radius around **13**. HINT log*P* calculations can be imported in Sybyl to derive hydropathic surface maps useful to visualize the non-covalent hydrophobic interactions of ligands and the binding domain of proteins. The contour map of the interaction between the binding domain and **13** was displayed with polar regions in red and hydrophobic regions in white. The HINT log*P* values for all compounds tested in this study were also calculated.

RESULTS AND DISCUSSION

The β-triketone natural products **2** and **4**−**7** and structural analogues **1**, **3**, **8**, **9**, **11**−**13**, and **17**−**19** (**Figure 1**) were synthesized for an earlier study examining the relationships of their structures to their antibacterial activity (*19*). These compounds contain a wide range of hydrophobic alkyl side chains attached to C-1′, and either tetramethyl, tetraethyl, or tetraprenyl substituents on the triketone ring (**Figure 1**). For the current work on the herbicidal activity of triketones, the new compounds **10** and **14**−**16** were synthesized and characterized. Compound **10**, with the β-triketone moiety modified but still containing a 1,3-diketone moiety, was prepared by simple methylation of **9**. NOESY NMR of **10** showed correlations between the methoxyl protons and the C-3′-methyl protons and the H-2′ and H-3′ protons on the flexible ethylene bridge.

The 1,3-diketone moiety was removed in compounds **15** and **16**. The oxidation of leptospermone **4** to give **15** was based on the reported reactions of another natural β-triketone, hyperforin (*34*). Several peroxidic reagents were tested to induce oxidative rearrangement, and it was found that suspending leptospermone **4** in dioxane and treating it with a high concentration of hydrogen peroxide gave a low yield (16%) of **15**. 2D NMR confirmed the proposed ester structure **15**, in particular an HMBC correlation between H-1 and C-1′. The presence of H-1 showed that the most stable form of ester **15** had nonconjugated C-2 and C-6 ketone groups, rather than the conjugated ketone−enol found in the β-triketones (*16*). Isoxazole **16** was obtained in good yield by treating β-triketone **9** with hydroxylamine, as per the method of Du Bois et al. (*35*) with spectroscopic data supporting the isoxazole structure. Compound **14**, with a single prenyl group on the ring, was prepared via monoprenyl phloroglucinol **20**, which was then permethylated.

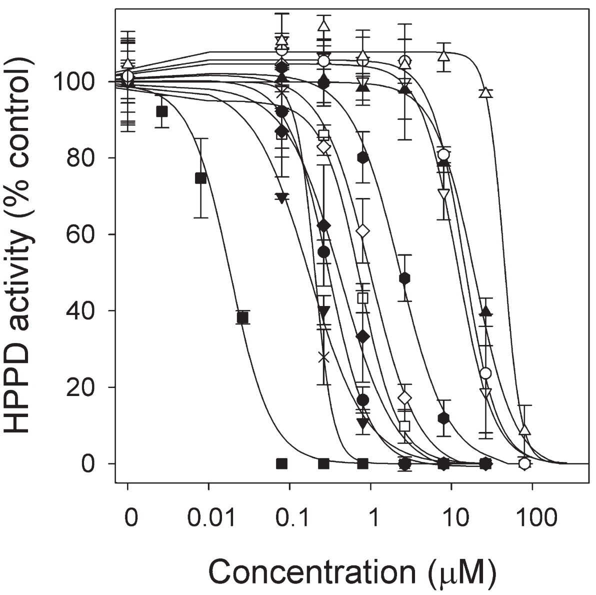

Figure 2. Inhibition of HPPD by triketones **2** (△), **4** (▽), **5** (○), **6** (□), **7** (◇), **12** (×), **3** (▲), **9** (▼), **13** (●), **11** (■), **10** (◆), and **14** (⬢). Each data point represents the mean of three independent experiments ± 1 SD. Compounds **1**, **8**, and **15**−**19** are not shown because their I_{50} values were >50 μM.

These triketones and related structures (**Figure 1**) were tested for their HPPD inhibitory activity as previously described (*25*). Dose−response curves against overexpressed and purified *A. thaliana* HPPD were obtained for all of the compounds (**Figure 2**), and I_{50} values were calculated using a four-parameter logistic function (**Table 1**). The results obtained with the leptospermone **4** and grandiflorone **6** synthesized in the laboratory (**Table 1**) were within experimental error of the results earlier reported for these compounds isolated from *L. scoparium* essential oil (*25*). Grandiflorone **6** was the most active of the naturally occurring β-triketones (I_{50} = 750 nM), which was closely followed by papuanone **7** (I_{50} = 960 nM). These levels of activity were close to that of the synthetic herbicide sulcotrione (I_{50} = 250 nM).

Grandiflorone **6** is present at low levels in some essential oils distilled from leaves of *L. scoparium* (*14*) and is the major component in essential oil from leaves of *L. morrisonii* (*17*). Accumulation of toxic secondary metabolites provides protection against herbivory and may also participate in allelopathy. In fact, the allelopathic properties of *Callistemon citrinus* were traced to the β-triketones it produced (*24*), which ultimately led to the discovery and development of the β-triketone synthetic herbicides (*7*).

The mechanism that enables *Leptospermum* species to be protected from these potent natural herbicides is not well understood. However, leaves of *Leptospermum* and other Myrtaceae species possess schizogenous cavities (*36*). These specialized structures, along with glandular trichomes and other glands, are often the site of synthesis and/or serve as a repository for bioactive natural products (*37*), thereby compartmentalizing these toxins and protecting the rest of the plant from autotoxic effects (*38*).

The synthetic compounds with no 1,3-diketone moiety, that is, the ester **15** and isoxazole **16**, were inactive (I_{50} > 50 μM; **Table 1**). This is consistent with the known requirement for the 1,3-diketone moiety to interact with the Fe^{2+} in the active site of HPPD. The O-methylated compound **10** retained this moiety and remained active (I_{50} = 410 nM), although to a lower degree than the parent β-triketone **9** (**Table 1**). Compounds **17**−**19** with bulky tetraprenyl or tetraethyl substituents on the triketone ring were inactive, whereas most of the tetramethyl compounds were active (**Table 1**). The monoprenyl-substituted **14** was active (I_{50} = 2,270 nM), but was 10 times less potent than the tetramethyl analogue **9**. Compound **14** has a chiral center at C-5 but was synthesized as a racemic mixture of enantiomers, which occurs as a 3:2 mixture of tautomers. The moderate inhibitory activity of this mixture indicated that one or more of these configurations interacted with the catalytic site of HPPD. Analysis of the binding domain, however, revealed that the space at the proximity of the Fe atom is limited, with the exception of a channel toward the bottom of the domain. Therefore, the bioactive form of **14** was presumed to be its C-5 carbon with an *R* absolute configuration (i.e., with the prenyl group β-oriented). Additionally, the binding domain could accommodate only the tautomeric form with the C-5 prenyl side chain pointing down. Therefore, this configuration of **14** was included in the data set used for the structure−activity relationship analysis.

The side chain on the β-triketones (R_1, **Figure 1**) had a major influence on the activity. For example, the presence of a simple methyl group (**1**) or cyclohexyl group (**8**) yielded inactive compounds, whereas the presence of a nonyl side chain (**11**) resulted in the most active compound in this study (I_{50} = 19 nM, **Table 1**). Other structure−activity work performed during the development of synthetic β-triketone herbicides also reported that compounds with short aliphatic groups on C-1′ had little to no activity (*24*).

In the previous work on the antibacterial structure−activity relationships (SAR) of β-triketones, there was a simple relationship between antibacterial potency and the calculated water−octanol partition coefficient (Clog *P*) (*19*). In that study, **12** with the undecyl side chain was the most active compound in the sample set. Compounds with higher or lower Clog *P* values were progressively less active (*19*). Previous works on the activity of natural products against plant HPPD also suggested that side-chain lipophilicity was also important in this biological system (*25*, *39*). However, Clog *P* values for the β-triketones in the present study showed that there was no simple relationship between this parameter and activity against HPPD (**Table 1**). For example, compound **8** with cyclohexyl ring attached to C-1′ has a Clog *P* similar to that of grandiflorone **6**, but it was at least 60 times less active against HPPD. HINT log *P* values (*40*) correlated closely with Clog *P* values (**Table 1**) and did not provide a better understanding of the contribution of log *P* to the activity of these compounds.

Therefore, 3D modeling techniques of the ligand/receptor interactions and CoMFA were used. The CoMFA method evaluates variations in steric and electronic field potentials of structural analogues that have been overlaid on a three-dimensional lattice and correlates these surfaces with biological activity using partial least-squares (PLS) analysis (*31*). The mathematical models obtained can be used to predict the activity of an analogue not included (leave-one-out) in the original data set or as a tool for visualizing SAR surfaces maps in three dimensions. CoMFA results include an r^2 value, which indicates how much of the data set's variation is accounted for by the model, and a cross-validated r^2 (q^2), which indicates how well biological activity is predicted for each compound by the other analogues in the data set (*31*). Experimentally, any model with a $q^2 > 0.5$ has a strong and statistically valid predictive power (*31*).

Structures were built and minimized in Sybyl and docked into a homology model of *A. thaliana* HPPD (*At*-HPPD) that had been developed previously (*25*). The coordinates of the protein−ligand interactions between the keto groups of the cocrystallized ligand and the Fe^{2+} ion in the catalytic domain NTBC were used to pre-position the compounds used this study. The coordinates of

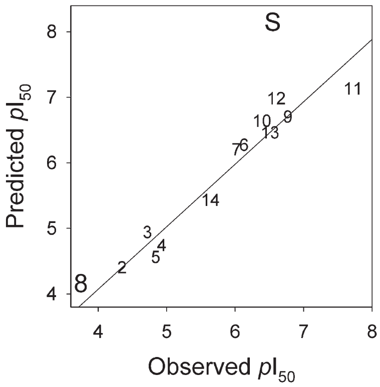

Figure 3. Observed and CoMFA predicted activities of β-triketones against HPPD. Cross-validated partial least-squares (PLS) analysis had an r^2 = 0.96, and the ability of the model to predict activity is q^2 = 0.63. The activities of sulcotrione **S** and **8**, which were not used to derive the CoMFA model, are shown in large type.

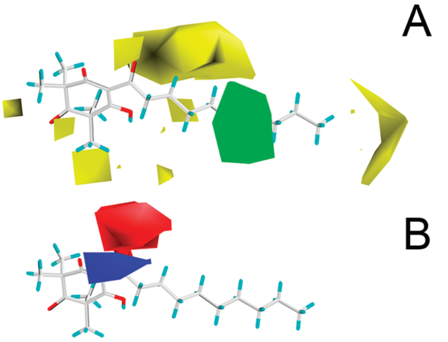

Figure 4. CoMFA maps of the β-triketones: (**A**) steric map where green areas indicate increase in steric bulk is favored and yellow areas indicate increase in steric bulk is not favored; (**B**) electrostatic map where blue areas indicate positive charge and H-bond donors are favored and negative charge and H-bond acceptors are not favored. Red areas indicate negative charge and H-bond acceptor are favored and positive charge and H-bond donors are not favored.

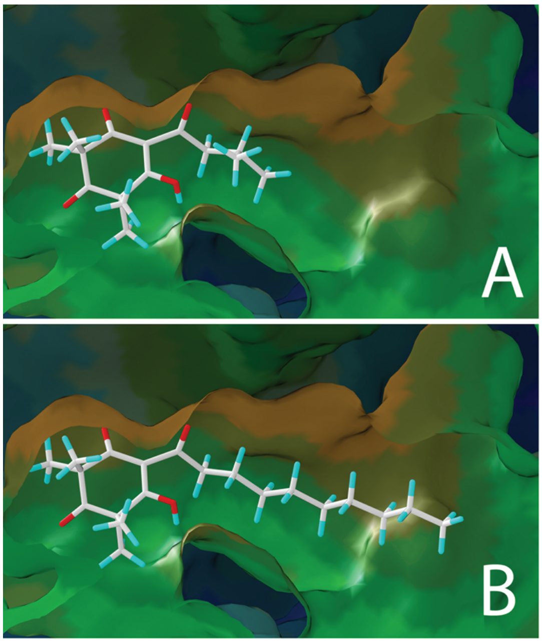

Figure 5. Binding mode of (**A**) leptospermone (**4**) and (**B**) **11** within the substrate binding domain of HPPD.

NTBC complexed with HPPD (*30*) were used instead of those of the pyrazole present in the *A. thaliana* HPPD crystal structure (*29*) because of the greater similarity between the triketones used in this study and NTBC than between the triketones and the pyrazole (see Figure S1 in the Supporting Information). Once pre-positioned in the catalytic site, the hydrophobic side chains were permitted to relax within the boundary of the binding domain to estimate their bioactive conformations and relative binding energies (**Table 1**).

The structures were then aligned on their common atoms within the triketone ring and subjected to CoMFA, which resulted in a strong linear relationship between the measured and predicted inhibitory activity, with an r^2 of 0.96 (**Figure 3**). The q^2 value of 0.63 suggests that the model can predict the activity of structurally related triketones. The standard error of regression (RSE) was near the expected noise level, indicating that the model was not overspecified. The CoMFA model indicates that 66% of the relationship was contributed by the steric energies of interaction, and 34% was due to electrostatic energies.

Compounds with large tetraethyl or tetraprenyl groups on the β-triketone ring (**17**−**19**) were not active because of steric hindrance near the catalytic site. The volume of the tetramethyl cyclic triketone moiety of compounds **1**−**12** (184.7 Å^3) is sufficiently small to fit within the pocket, whereas the volumes of **17** (254.2 Å^3) and of **18** and **19** (438.3 Å^3) prohibit binding (**Table 1**). The inability of larger β-triketones to fit within this space was reflected by their exceedingly high calculated binding energies (**Table 1**). CoMFA maps identified that the presence of bulky substituents on the ring structure had a negative impact on the activity of the compounds (yellow surfaces in **Figure 4A**). This is consistent with the observation that the volume of the binding domain can accommodate the β-triketones from the tetramethyl homologous series, but it is not large enough for triketones decorated with bulkier side chains (**17**−**19**).

On the other hand, the calculated binding energies of **15** and **16** suggest that the compounds could fit within the substrate binding domain (**Table 1**), but were not active due to the absence of the 1,3-diketone moiety (**Figure 1**) that is necessary to form coordinated octahedral complexes with the Fe^{2+} ion and three strictly conserved active site residues in the catalytic site (*25*, *41*). The CoMFA map identifies this region as important for electrostatic interactions (see blue and red surfaces surrounding the 1,3-diketone moiety in **Figure 4B**).

The relatively low binding energies of the remaining β-triketones (**Table 1**) suggest that they fit well within the substrate binding domain regardless of the size or length of the R$_1$ side chain (**Figure 5**). The presence of a cyclohexyl ring (or benzyl ring) does not preclude activity, as observed with **3**, **6**, and **9**, but its proximity to the C-1′ of the triketone ring has a strong effect on activity. The structure−activity relationship between **8**, **3**, **6**, **10**, and **9** clearly shows that increasing the distance between a side-chain ring and C-1′ improves activity (**Table 1**).

The I_{50} value of **8** could not be calculated from the dose−response curve because the highest concentration tested (100 μM) provided only 35% inhibition of HPPD. However, the CoMFA model predicted an I_{50} of 69 μM for **8**, which is a reasonable approximation of its low inhibitory activity against HPPD (see estimated position of **8** in **Figure 3**). The CoMFA map identifies the region proximal to the C-1′ of the triketone ring as particularly sensitive to steric hindrance (yellow area in **Figure 4A**). At the other end of the activity range, the CoMFA model predicted the I_{50} of sulcotrione to be 7 nM, whereas its measured activity I_{50} against HPPD was 250 nM (see position of **S** in **Figure 3**). This overestimation of the activity of sulcotrione may be due to the fact that none of the structures used to derive

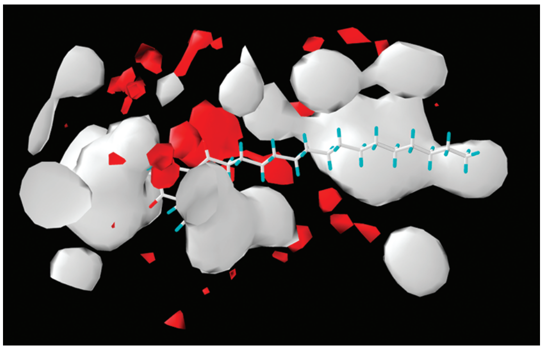

Figure 6. HINT polar/hydrophobic surface map of the catalytic site and binding domain of HPPD. Red surfaces represent polar areas and white surfaces represent hydrophobic areas contributed by the amino acids lining the substrate binding domain. Note the highly hydrophobic region surrounding the aliphatic tail of the inhibitor (**13**).

the CoMFA model had the chloro and methane sufonyl groups built into this synthetic herbicide. The presence of strong electron-withdrawing groups para on the phenyl ring of synthetic herbicidal compounds increased activity by 40-fold (*12*, *42*).

The biological activities **12** and **13** were lower than that of **11**, which has a shorter and less lipophilic side chain. Analysis of the relationship between log *P* and activity could not account for this, but the three-dimensional CoMFA approach successfully predicted the activity of these compounds (**Figure 3**). The steric CoMFA map identified this by the presence of a yellow area toward the end of the hydrophobic tail (**Figure 4A**).

Finally, the substrate binding domain of HPPD consists of a lipophilic region lined with Met314, Pro315, Pro318, Phe360, Phe371, Phe403, Leu405, and Phe407 (**Figure 6**). This domain favors the binding of ligands with lipophilic moieties. For this reason, triketones with long hydrophobic side chains tend to have higher inhibitory activity than those with short side chains. This is consistent with previous observations that the biological activity of both natural and synthetic β-triketones is greatly affected by the nature of any side chain attached to the triketones (*24*, *25*, *43*).

Synthetic triketone-based HPPD inhibitors were discovered following a study on the phytotoxic properties of leptospermone **4** (*24*). The modeling of β-triketone interactions with plant HPPD reported above has yielded important information to further understand the basis for inhibition by these natural product derived herbicides. Although the physicochemical properties of the β-triketones used in this study are suboptimal when compared to those of the synthetic products commercially available, work is underway to determine the in vivo activity of these molecules and the potential use of the natural β-triketones as herbicides in organic agriculture.

ABBREVIATIONS USED

HPPD, *p*-hydroxyphenylpyruvate dioxygenase; 4-HPP, 4-hydroxyphenylpyruvate; HGA, homogentisic acid; NTBC, 2-[2-nitro-4-(trifluoromethyl)benzoyl]-1,3-cyclohexanedione.

ACKNOWLEDGMENT

We thank E. Burgess and S. B. Watson for their technical assistance, B. Clark and I. Stewart for MS, and M. Thomas for assistance with NMR. We are also grateful to Rhône-Poulenc for the generous gift of the recombinant HPPD.

Supporting Information Available: Structures of leptospermone, NTBC, and DAS645. This material is available free of charge via the Internet at http://pubs.acs.org.

LITERATURE CITED

(1) Que, L.; Ho, R. Y. N. Dioxygen activation by enzymes with mononuclear non-heme iron active sites. *Chem. Rev.* **1996**, *96*, 2607–2624.

(2) Crouch, N. P.; Adlington, R. M.; Baldwin, J. E.; Lee, M.-H.; MacKinnnon, C. H. A mechanistic rationalisation for the substrate specificity of recombinant mammalian 4-hydroxyphenylpyruvate dioxygenase. *Tetrahedron* **1997**, *53*, 6993–7010.

(3) Pascal, R. A.; Oliver, M. A.; Chen, Y. C. J. Alternate substrates and inhibitors of bacterial 4-hydroxyphenylpyruvate dioxygenase. *Biochemistry* **1985**, *24*, 3158–3165.

(4) Norris, S. R.; Barrette, T. R.; DellaPenna, D. Genetic dissection of carotenoid synthesis in *Arabidopsis* defines plastoquinone as an essential component of phytoene desaturation. *Plant Cell* **1995**, *7*, 2139–2149.

(5) Pallett, K. E.; Little, J. P.; Sheekey, M.; Veerasekaran, P. The mode of action of isoxaflutole I. Physiological effects, metabolism, and selectivity. *Pestic. Biochem. Physiol.* **1998**, *62*, 113–124.

(6) Schulz, A.; Ort, O.; Beyer, P.; Kleinig, H. SC-0051, a 2-benzoyl-cyclohexane-1,3-dione bleaching herbicide, is a potent inhibitor of the enzyme *p*-hydroxyphenylpyruvate dioxygenase. *FEBS Lett.* **1993**, *318*, 162–166.

(7) Lee, D. L.; Prisbylla, M. P.; Cromartie, T. H.; Dagarin, D. P.; Howard, S. W.; Provan, W. M.; Ellis, M. K.; Fraser, T.; Mutter, L. C. The discovery and structural requirements of inhibitors of *p*-hydroxyphenylpyruvate dioxygenase. *Weed Sci.* **1997**, *45*, 601–609.

(8) Viviani, E.; Little, J. P.; Pallett, K. E. The mode of action of isoxaflutole II. Characterization of the inhibition of carrot 4-hydroxyphenylpyruvate dioxygenase by the diketonitrile derivative of isoxaflutole. *Pestic. Biochem. Physiol.* **1998**, *62*, 125–134.

(9) Schultz, T. W.; Bearden, A. P. Structure−toxicity relationships for selected naphthoquinones to *Tetrahymena pyriformis*. *Bull. Environ. Contam. Toxicol.* **1998**, *61*, 405–410.

(10) Senseman, S. A. *Herbicide Handbook*, 9th ed.; Weed Science Society of America: Lawrence, KS, 2007; p 458.

(11) Williams, M. M.; Pataky, J. K. Genetic basis of sensitivity in sweet corn to tembotrione. *Weed Sci.* **2008**, *56*, 364–370.

(12) Lee, D. L.; Knudsen, C. G.; Michaely, W. J.; Chin, H.-L.; Nguyen, N. H.; Carter, C. G.; Cromartie, T. H.; Lake, B. H.; Shribbs, J. M.; Fraser, T. The structure−activity relationships of the triketone class of HPPD herbicides. *Pestic. Sci.* **1998**, *54*, 377–384.

(13) Gray, R. A.; Tseng, C. K.; Rusay, R. J. 1-Hydroxy-2-(alkylketo)-4,4,6,6-tetramethyl cyclohexen-3,5-dione herbicides. U.S. Patent 4,227,919, 1980.

(14) Douglas, M. H.; van Klink, J. W.; Smallfield, B. M.; Perry, N. B.; Anderson, R. E.; Johnstone, P.; Weavers, R. T. Essential oils from New Zealand manuka: triketone and other chemotypes of *Leptospermum scoparium*. *Phytochemistry* **2004**, *65*, 1255–1264.

(15) Hellyer, R. O. The occurrence of β-triketones in the steam-volatile oils of some myrtaceous australian plants. *Aust. J. Chem* **1968**, *21*, 2825–2828.

(16) van Klink, J. W.; Brophy, N. B.; Perry, N. B.; Weavers, R. T. Triketones from myrtaceae: isoleptospermone from *Leptospermum scoparium* and papuanone from *Corymbia dallachiana*. *J. Nat. Prod.* **1999**, *62*, 487–489.

(17) Brophy, J. J.; Goldsack, R. J.; Bean, A. R.; Forster, P. I.; Lepschi, B. J. Leaf essential oils of the genus *Leptospermum* (Myrtaceae) in eastern Australia. Part 6. *Leptospermum polygalifolium* and allies. *Flavour Fragrance J.* **2000**, *15*, 271–277.

(18) Rubinov, D. B.; Rubinova, I. L.; Akhrem, A. A. 2-Acylcycloalkane-1,3-diones. *Chem. Nat. Compd.* **1995**, *31*, 537–559.

(19) van Klink, J. W.; Larsen, L.; Perry, N. B.; Weavers, R. T.; Cook, G. M.; Bremer, P. J.; MacKenzie, A. D.; Kirika, T. Triketones active against antibiotic-resistant bacteria: synthesis, structure−activity relationships, and mode of action. *Bioorg. Med. Chem.* **2005**, *13*, 6651–6662.

(20) Christoph, F.; Kaulfers, P.-M.; Stahl-Biskup, E. A comparative study of the *in vitro* antimicrobial activity of tea tree oils with special reference to the activity of β-triketones. *Planta Med.* **2000**, *66*, 556–560.

(21) Spooner-Hart, R. N.; Basta, A. H. Pesticidal compositions containing β-diketones and β-triketones from essential oils. *Pct. Int. Appl.* Coden PIXXD2 WO 2002089587, AI 20021114, CAN 137:347894, AN 2002:868663, 2002; 88 pp.

(22) Christoph, F.; Kubeczka, K. H.; Stahl-Biskup, E. The composition of commercial manuka oils from New Zealand. *J. Essent. Oil Res.* **1999**, *11*, 705–710.

(23) Reichling, J.; Koch, C.; Stahl-Biskup, E.; Sojka, C.; Schnitzler, P. Virucidal activity of a β-triketone-rich essential oil of *Leptospermum scoparium* (manuka oil) against HSV-1 and HSV-2 in cell culture. *Planta Med.* **2005**, *71*, 1123–1127.

(24) Knudsen, C. G.; Lee, D. L.; Michaely, W. J.; Chin, H.-L.; Nguyen, N. H.; Rusay, R. J.; Cromartie, T. H.; Gray, R.; Lake, B. H.; Fraser, T. E. M.; Cartwright, D. Discovery of the triketone class of HPPD inhibiting herbicides and their relationship to naturally occurring β-triketones. In *Allelopathy in Ecological Agriculture and Forestry*; Narwal, S. S., Ed.; Kluwer Academic Publishers: Dordrecht, The Netherlands, 2000; pp 101−111.

(25) Dayan, F. E.; Duke, S. O.; Sauldubois, A.; Singh, N.; McCurdy, C.; Cantrell, C. L. *p*-Hydroxyphenylpyruvate dioxygenase is a herbicidal target site for β-triketones from *Leptospermum scoparium. Phytochemistry* **2007**, *68*, 2004–2014.

(26) Garcia, I.; Rodgers, M.; Pepin, R.; Hsieh, T.-Z.; Matringe, M. Characterization and subcellular compartmentation of recombinant 4-hydroxyphenylpyruvate dioxygenase from *Arabidopsis* in transgenic tobacco. *Plant Physiol.* **1999**, *119*, 1507–1516.

(27) Ritz, C.; Streibig, J. C. Bioassay analysis using R. *J. Statist. Soft* **2005**, *12*, 1–22.

(28) R-Development-Core-Team. *R: A Language and Environment for Statistical Computing*, 2.2.1; R Foundation for Statistical Computing: Vienna, Austria, 2005.

(29) Yang, C.; Pflugrath, J. W.; Camper, D. L.; Foster, M. L.; Pernich, D. J.; Walsh, T. A. Structural basis for herbicidal inhibitor selectivity revealed by comparison of crystal structures of plant and mammalian 4-hydroxyphenylpyruvate dioxygenases. *Biochemistry* **2004**, *43*, 10414–10423.

(30) Brownlee, J. M.; Johnson-Winters, K.; Harrison, D. H.; Moran, G. R. Structure of the ferrous form of (4-hydroxyphenyl)pyruvate dioxygenase from *Streptomyces avermitilis* in complex with the therapeutic herbicide, NTBC. *Biochemistry* **2004**, *43*, 6370–6377.

(31) Cramer, R. D. I.; Patterson, D. E.; Bunce, J. D. Comparative molecular field analysis (CoMFA). Effect of shape of binding of steroids to carrier proteins. *J. Am. Chem. Soc.* **1988**, *110*, 5959–5967.

(32) Halgren, T. A. Maximally diagonal force constants in dependent angle-bending coordinates. II. Implications for the design of empirical force fields. *J. Am. Chem. Soc.* **1990**, *112*, 4723–4728.

(33) Kellogg, G. E.; Semus, S. F.; Abraham, D. J. HINT: a new method of empirical hydrophobic field calculation for CoMFA. *J. Comput.-Aid. Mol. Des.* **1991**, *5*, 545–552.

(34) Verotta, L.; Lovaglio, E.; Sterner, O.; Appendino, G.; Bombardelli, E. Oxidative fragmentation of the bridged β-triketone core of hyperforin. *Eur. J. Org. Chem.* **2004**, *6*, 1193–1197.

(35) DuBois, G. E.; Crosby, G. A.; Stephenson, R. A. Dihydrochalcone sweeteners—a study of the atypical temporal phenomena. *J. Med. Chem.* **1981**, *24*, 408–428.

(36) List, S.; Brown, P. H.; Walsh, K. B. Functional anatomy of the oil glands of *Melaleuca alternifolia* (Myrtaceae). *Aust. J. Bot.* **1995**, *43*, 629–641.

(37) Dayan, F. E.; Duke, S. O. Trichomes and root hairs: natural pesticide factories. *Pestic. Outlook* **2003**, *4*, 175–178.

(38) Sirikantaramas, S.; Yamakazi, M.; Saito, K. Mechanisms of resistance to self-produced toxic secondary metabolites in plants. *Phytochem. Rev.* **2008**, *7*, 467–477.

(39) Meazza, G.; Scheffler, B. E.; Tellez, M. R.; Rimando, A. M.; Nanayakkara, N. P. D.; Khan, I. A.; Abourashed, E. A.; Romagni, J. G.; Duke, S. O.; Dayan, F. E. The inhibitory activity of natural products on plant *p*-hydroxyphenylpyruvate dioxygenase. *Phytochemistry* **2002**, *59*, 281–288.

(40) Kellogg, G. E.; Abraham, D. J. Hydrophobicity: is LogPo/w more than the sum of its parts?. *Eur. J. Med. Chem.* **2000**, *35*, 651–661.

(41) Kakidani, H.; Hirai, K. Three-dimensional modeling of plant 4-hydroxyphenylpyruvate dioxygenase, a molecular target of triketone-type herbicides. *J. Pestic. Sci.* **2003**, *28*, 409–415.

(42) Ellis, M. K.; Whitfield, A. C.; Gowans, L. A.; Auton, T. R.; Provan, W. M.; Lock, E. A.; Lee, D. L.; Smith, L. L. Characterization of the interaction of 2-[2-nitro-4-(trifluoromethyl)benzoyl]-4,4,6,6-tetramethylcyclohexane-1,3,5-trione with rat hepatic 4-hydroxyphenylpyruvate dioxygenase. *Chem. Res. Toxicol.* **1996**, *9*, 24–27.

(43) Huang, M.; Yang, D.-Y.; Shang, Z.; Zou, J.; Yu, Q. 3D-QSAR studies on 4-hydroxyphenylpyruvate dioxygenase inhibitors by comparative molecular field analysis (CoMFA). *Bioorg. Med. Chem. Lett.* **2002**, *12*, 2271–2275.

Received September 12, 2008. Revised manuscript received April 21, 2009. This research was supported in part by the New Zealand Foundation for Research, Science and Technology.